Soil-water carrying capacity of revegetation species in the Loess Plateau, China

Xiaoxu Jia[a,b], Dongxue Yu[a,b], Yu Zhang[c], Baoni Xie[d], Yuanjun Zhu[e], Andrew Binley[f], Mingan Shao[a,b*]

[a]Key Laboratory of Ecosystem Network Observation and Modeling, Institute of Geographical Sciences and Natural Resources Research, Chinese Academy of Sciences, Beijing 100101, China

[b]College of Resources and Environment, University of Chinese Academy of Sciences, Beijing 100190, China

[c]College of Resource and Environmental Sciences, Hebei Normal University, Shijiazhuang 050024, China

[d]School of Land Resources and Urban and Rural Planning, Hebei GEO University, Shijiazhuang 050031, China

[e]State Key Laboratory of Soil Erosion and Dryland Farming on the Loess Plateau, Northwest A&F University, Yangling 712100, China

[f]Lancaster Environment Centre, Lancaster University, Bailrigg, Lancaster, LA1 4YQ, UK

*Correspondence: Ming'an Shao (Prof.)

Key Laboratory of Ecosystem Network Observation and Modeling, Institute of Geographical Sciences and Natural Resources Research, Chinese Academy of Sciences, Beijing 100101, China

Email: shaoma@igsnrr.ac.cn

Abstract: Re-vegetation is a necessary control measure of soil erosion in the Loess Plateau. However, excessive re-vegetation can aggravate soil water shortage, which can in turn threaten the health and services of restored ecosystems. An optimal plant cover or biomass (i.e., soil-water carrying capacity for vegetation, SWCCV) is important for regional water balance, soil protection and vegetation sustainability. The objective of this study was to determine the spatial distribution of SWCCV for three non-native tree (*Robinia pseudoacaia*), shrub (*Caragana korshinskii*) and grass (*Medicago sativa*) species used in the re-vegetation of the Loess Plateau. The dynamics of actual evapotranspiration (AET), net primary productivity (NPP) and leaf area index (LAI) were simulated using a modified Biome-BGC (Bio-Geochemical Cycles) model. Soil and physiological parameters required by the model were validated using field-observed AET for the three plant species at six sites in the study area. The validated model was used to simulate the dynamics of AET, NPP and LAI for the three plant species at 243 representative sites in the study area for the period 1961–2014. The results show that spatial distributions of mean AET, NPP and LAI generally increased from northwest to southeast, much the same as mean annual precipitation (MAP) gradient. In terms of maximum LAI, the ranges of optimal plant cover were 1.1–3.5 for *R. pseudoacaia*, 1.0–2.4 for *C. korshinskii* and 0.7–3.0 for *M. sativa*. The corresponding SWCCV, expressed as NPP were 202.4–616.5, 83.7–201.7 and 56.3–253.0 g C m^{-2} yr^{-1}. MAP, mean annual temperature, soil texture and elevation were the main variables driving SWCCV under the plant species; explaining over 86% of the spatial variations in mean NPP in the study area. Further

re-vegetation therefore needs careful reconsideration under the prevailing climatic, soil and topographic conditions. The results of the study provide a re-vegetation threshold to guide future re-vegetation activities and to ensure a sustainable eco-hydrological environment in the Loess Plateau.

Keywords: Plant cover, carrying capacity, re-vegetated soil, Biome-BGC model, Loess Plateau

1. Introduction

Vegetation restoration is one of the principal measures for improving the ecological environment and for conserving both soil and water in fragile ecosystems that are easily destroyed by human disturbances or severe environmental conditions. Re-vegetation of degraded lands is promoted globally due to the numerous benefits it has, including carbon sequestration (Eaton et al., 2008), bio-conservation (Chirino et al., 2006; Jia et al., 2011), sediment reduction (Wang et al., 2016) and regulation of hydro-climatic conditions (Yaseef et al., 2009; McVicar et al., 2010; Feng et al., 2012). However, excessive planting of non-native species will increase soil water deficit and limit the carrying capacity of artificial vegetation in arid and semiarid regions, which in turn will adversely affect the succession of vegetation. Balancing plant cover/biomass and soil water availability in water-scarce regions is therefore critical for sustainable development of restored ecosystems (Chen et al., 2015; Feng et al., 2016; Mo et al., 2016; Zhang et al., 2018).

The Loess Plateau (LP) of China is in the upper and middle reaches of the

Yellow River, and has an area of 640 000 km^2 and with the most severe soil erosion in the world (Shi and Shao, 2000). A series of vegetation restoration measures were implemented by the China's Central Government at the end of the 1990s to convert croplands to forests, shrubs and grass as a way of mitigating soil erosion and improving ecosystem services in the region. Since then, vegetation cover has dramatically increased on the plateau from 31.6% in 1999 to 59.6% in 2013. Also annual sediment discharge into the Yellow River has sharply dropped from 1.6 to 0.2 Gt (Chen et al., 2015). For the period 1998–2010, Wang et al. (2016) observed 21% decline in sediment load in 12 main sub-catchments on the plateau; which was attributed to massive afforestation drive in the region. Although soil erosion has been effectively controlled by the restoration of vegetation, excessive introduction of exotic plant species (e.g., *Robinia pseudoacaia*, *Caragana korshinskii*, *Hippophae rhamnoides* and *Medicago sativa*, etc.) along with high planting density has caused the formation of dry soil layer (DSL) in the region (Jia et al., 2017a, b; Zhang et al., 2018). This is a severe obstacle to sustainable land use and water cycle in the soil-plant-atmosphere continuum as it limits water exchange between the upper soil layers and groundwater (Wang et al., 2011; Turkeltaub et al., 2018).

The concept of soil-water carrying capacity for vegetation (SWCCV) was introduced to quantify the maximum vegetation density or biomass in China's LP that can be sustained without soil desiccation (Guo and Shao, 2004; Xia and Shao, 2008; Liu and Shao, 2015). It was developed and defined as the maximum cover or biomass of a plant community at which soil-water consumption is equal to the soil-water supply in the root zone under given climatic condition, soil texture and management practice (Shao et al., 2018). When plant cover or biomass exceeds the maximum limit of SWCCV, a series of consequences that restrict plant growth and aggravate soil water scarcity along with soil desiccation is ensured (Xia and Shao, 2008; Fu et al., 2012; Zhang et al., 2015a). Therefore, it is important to quantify SWCCV for dominant non-native plant species to avoid soil desiccation and to ensure sustainable vegetation recovery.

A number of studies have been done on SWCCV of different plant species and at different spatial and temporal scales using field data and model simulations (Guo and Shao, 2004; Xia and Shao, 2008; Fu et al., 2012; Liu and Shao, 2015; Zhang et al., 2015a). Using conceptual water balance model, Guo and Shao (2004) developed an empirical mathematical model from which SWCCV was determined for 8115 ha^{-1} of *C. korshinskii* plantation in the semi-arid hilly area of China's LP. Xia and Shao (2008) developed a physically-based model for calculating optimal plant cover (with *C. korshinskii* and *Salix psammophila* as case study) using 2–3 years of climate data in a small watershed in the northern region of China's LP. Liu and Shao (2015) assessed the consumption process of soil water with the growth of *C. korshinskii* and *M. sativa* and the optimal carrying capacity of each using the one-dimensional Simultaneous Heat and Water Transfer (SHAW) model. The estimated SWCCVs corresponding with maximum biomass production were 4800 kg ha^{-1} for *C. korshinskii* and 1380 kg ha^{-1} for *M. sativa*. Eagleson's ecohydrological optimality method (Eagleson, 2002) was also used to determine the optimal canopy cover in Horqin Sands of China (Mo et al.,

2016) and the Northeast China Transect (Cong et al., 2017). Most other studies on optimal carrying capacity are based on field experiments that last 1–3 years and therefore not adequate to fully represent long-term variability of SWCCV due to large fluctuations in annual precipitation in China's LP region. Therefore, it is necessary to consider variations in long-term climatic conditions in the study of SWCCV (Shao et al., 2018). It is also good to assume that the optimal carrying capacity is equal to the long-term average of plant cover/biomass in a given area (Zhang et al., 2015a).

Considering the widespread occurrence and severity of DSL and the negative effects it has on hydro-ecological environment in China's LP, more information is needed on regional spatial distribution of SWCCV under dominant non-native plant species in the region. This could guide policy decisions and vegetation restoration strategies for optimized soil water management. Zhang et al. (2015a) estimated the spatial distributions of optimal plant cover for *R. pseudoacacia* and *H. rhamnoides* along a precipitation gradient in the central region of China's LP using eco-physiological and bio-geochemical processes model, Biome-BGC (White et al., 2000; Thornton et al., 2002). This model is widely used to simulate daily, monthly and annual water, carbon and nitrogen storages and fluxes in and out of terrestrial ecosystems. Due largely to the lack of measured regional soil data, however, there are currently no reports addressing the spatial distributions of SWCCV for the dominant non-native tree, shrub and grass species in the whole China's LP. To accurately simulate regional spatial distributions of SWCCV using the modified Biome-BGC model, data on the hydraulic properties of soil within the 5 m profile were collected in a field survey at 243 sites along with long-term (1961–2014) daily climate data across China's LP region.

Thus, the specific objectives of this study were to: 1) estimate optimal plant cover (from maximum leaf area index — LAI) and SWCCV (expressed as net primary productivity — NPP) for three most dominant non-native tree (*R. pseudoacacia*), shrub (*C. korshinskii*) and grass (*M. sativa*) species at 243 representative sites using modified Biome-BGC model; 2) develop spatial distributions of SWCCV for the three plant species across China's LP region through kriging interpolation; and 3) determine the main variables contributing to the spatial variability of SWCCV in the study area. This information should be useful in drawing recommendations for vegetation construction in China's LP region to balance the conflict between scarce soil water and soil conservation through re-vegetation.

2. Materials and methods

2.1. Study area and representative plants

The study was conducted in China's LP; a region in the upper through middle reaches of Yellow River (100.90°E–114.55°E and 33.72°N–41.27°N) (Fig. 1) and characterized by 30–200 m thick loess soil (Zhu et al., 2018). The region covers an area of ~640 000 km^2 and has a semi-arid to sub-humid climate. The range of the mean annual precipitation for 1961–2014 is 200–700 mm; lowest in the northwest and highest in the southeast. About 55–78% of the precipitation falls in June through September. The range of the mean annual temperature is 3.6–14.3 °C; also lowest in the northwest and highest in the southeast. The soil is mainly of loess and it is sandy in texture in the northwest and clayey in the southeast.

To control soil and water erosion and to restore the ecosystem, several large-scale vegetation restoration campaigns (including the Grain-for-Green Program — GFGP) were initiated by the China's Central Government at the end of the 1990s to reconvert croplands into forests, shrubs and grass across the plateau. The LP sub-region with continuous loess soil was chosen as the study area (Fig .1) because it is the main implementation zone of GFGP, so done to the control soil erosion. The region covers a total area of 430 000 km^2 and includes all the main regional climatic conditions (arid, semi-arid and sub-humid), soil texture (silt-clay, silt-clay-loam, silt-loam, loam, sand-loam and loam-sand), vegetation types (tree, shrub and grass) and geomorphic landforms (large flat surfaces with little or no erosion, ridges, basins, hills and gullies). The depth to groundwater in the study area is generally 30–100 m (Jia et al., 2017a; Turkeltaub et al., 2018) and the limited precipitation is the primary source of recharge and water for plant growth.

Various non-native plant species (including *Robinia pseudoacacia*, *Pinus tabuliformis*, *Populus*, *Platycladus orientalis*, *Firmiana platanifolia*, *Caragana korshinskii*, *Malus pumila*, *Armeniaca sibirica*, *Ziziphus jujube*, *Hippophae rhamnoides* and *Medicago sativa*) have been introduced in China's LP under vegetation restoration drive. The most common tree, shrub and grass species used in the restoration drive are *R. pseudoacacia* (black locust), *C. korshinskii* (peashrub) and *M. sativa* (alfalfa), which are exotic nitrogen-fixing species. These non-native plant species are widely used because of their strong drought resistance, high survival rate, soil fertility improvement and fast growth rate (Li et al., 1996; Cheng and Wan, 2002; Jia et al., 2017a).

2.2. Biome-BGC model description

Biome-BGC is a one-dimensional mechanistic biogeochemical model that can simulate daily, monthly and annual carbon, nitrogen and water cycles using prescribed soil and meteorological conditions (White et al., 2000; Thornton et al., 2002). It represents one point in space with carbon, nitrogen and water fluxes and storages normalized for a unit area. A study area is divided into cells and simulations performed independently for each cell in the area. The model provides complete parameters settings for main plant types, including deciduous broadleaf, shrub and grass (White et al., 2000). Carbon processes include autotrophic respiration, separated into growth and maintenance respiration, photosynthesis (for both sunlit and shaded leaves), decomposition, allocation and mortality. Gross primary productivity (GPP) is simulated with the Farquhar photosynthesis model (Farquhar et al., 1980) and NPP calculated as GPP minus maintenance respiration (a Q_{10} model) and growth respiration (a constant fraction of GPP). LAI is estimated as a function of the amount of leaf carbon, one of multiple vegetation state variables updated every day based on estimated fluxes. Water processes include canopy interception of rainfall, snow melt and sublimation, canopy evapotranspiration, soil evaporation and water outflow due to water in excess of field capacity. The water sub-model of Biome-BGC is very simple, and it calculates only daily water outflow from the soil when soil water content exceeds field capacity (Thornton et al., 2002). Huang et al. (2013) modified the original sub-routine by introducing a physically-based equation (i.e., the one-dimensional Richards' equation), to simulate soil water movement with root water uptake under limited water conditions. The modified Biome-BGC model was used in this study. Further details on the modification and evaluation of the water flow sub-model of Biome-BGC are documented by Huang et al. (2013). Further descriptions and equations of Biome-BGC are documented by White et al. (2000) and Thornton et al. (2002).

2.3. Model evaluation

Continuous measurements of LAI or NPP for the three plants were not available for the study site. However, previous studies show that NPP is linearly related with AET (Schimel et al., 1997; Bond-Lamberty et al., 2009), indicating that the modified Biome-BGC model also simulates NPP if it accurately simulates AET. Consequently, the modified Biome-BGC model was evaluated by comparing the simulated AET with AET determined by a water balance equation based on precipitation, runoff and soil water content (SWC) — see Eq. (1) below. The water balance approach is a common and reliable method of estimation of ET when soil water and precipitation are available (Palmroth et al., 2010). Soil water storage for *R. pseudoacacia* in Heshui, Guyuan, Changwu, An'sai and Dingxi is available for the periods 2003–2006 (Zhao, 2012), 1988–1999 (Cheng and Wan, 2002), 2011–2014 (Zhang et al., 2015b), 1982–1986 (Yang and Yang, 1989) and 2009–2013 (Jian et al., 2015). Monthly soil water storage for *C. korshinskii* in Dingxi is available for the period 2009–2013 (Jian et al., 2015). Measured AET for *M. sativa* in Changwu is available for the period 1986–2001 (Li and Huang, 2008). In addition, SWC and runoff data for *C. korshinskii* and *M. sativa* in Shenmu were measured for 2004–2014. Monthly volumetric SWC was measured during May to October each year to the depth of 500 cm at 20 cm intervals using calibrated neutron probe. All the measured and collected soil water data during the growing season at different sites in the study area were used to calculate AET as follows:

$$AET = P - R + \Delta W \quad (1)$$

where AET is actual evapotranspiration (mm); P is precipitation (mm); R is runoff (mm); and ΔW is change in soil water storage (mm) at start and end of growing season (May-October) in the 0–500 cm soil layer.

2.4. Determination of SWCCV

The modified Biome-BGC model was used to simulate annual variations in AET, LAI and NPP for three dominant non-native tree, shrub and grass species at the 243 sites across the LP during the period 1961-2014. Because the determination of optimal carrying capacity of vegetation considers variations in long-term climatic conditions, SWCCV for the three plant species was assumed to be equal to plant cover (derived from LAI) or biomass production (derived from NPP) and averaged for period under investigation. Since LAI increases during growing season, the maximum value for each year was used to represent the optimal soil-water carrying capacity of vegetation during that year.

2.5. Data sources

Inputs needed for the Biome-BGC model are as follows: 1) daily meteorological series (minimum and maximum air temperature, average air temperature, precipitation, humidity, solar radiation and day length); 2) site physical properties (e.g., latitude, longitude, elevation, slope, aspect, soil hydraulic parameters and rooting depth); and 3) eco-physiological parameters (e.g., carbon to nitrogen ratio and maximum stomatal conductance).

2.5.1. Meteorological parameters

In situ measurements of daily temperature (°C), relative humidity (%), precipitation (mm) and wind speed (m s^{-1}) were provided by the China Meteorology Administration for 213 meteorological stations distributed within and around the study area (Fig. 1). These data were interpolated using the thinplate smoothing spline method (Hartkamp et al., 1999; Liu et al., 2008) to build 1-km spatial resolution maps for the period 1961–2014. The maximum and minimum air temperatures, humidity and precipitation were used to calculate solar radiation, daylight average partial pressure of water vapor and day length through MT-CLIM (Thornton et al., 2000). The study area was divided into three rainfall zones: the northern zone with mean annual precipitation (MAP) <450 mm, the central zone with MAP of 450–550 mm, and the southern zone with MAP >550 mm (Li et al., 2008); which allows for comparison of the effects of rainfall on SWCCV for the three plant species.

2.5.2. Soil hydraulic parameters

To accurately determine spatial variations in soil hydraulic parameters in the region, an intensive soil sampling strategy was devised. Adjacent sampling sites were ~40 km apart and a total of 243 representative sampling sites were used across the LP region (Fig. 2). A GPS receiver was used to determine the latitude, longitude and elevation of each site, while site slope and aspect were determined using a geological compass. Further information concerning the soil sampling strategy and data collection is also documented by Zhao et al. (2016).

Undisturbed soil cores were excavated at the 0–10, 10–20 and 20–40 cm depths to measure saturated hydraulic conductivity (K_s), saturated SWC (θ_s) and bulk density (BD) at each site. In addition, disturbed soil samples were collected using a soil auger for the 0–10, 10–20, 20–40, 40–60, 60–80, 80–100, 100–150, 150–200, 200–300, 300–400 and 400–500 cm soil layers for soil particle distribution analyses. The soil hydraulic parameters required for the modified Biome-BGC model included K_s, θ_s, residual SWC (θ_r) and the van Genuchten model shape parameters (α and n). K_s was determined using the constant-head method (Klute and Dirksen, 1986) and BD determined from volume-dry mass relationship for each core sample. Soil retention curves and unsaturated hydraulic conductivity were estimated by the van Genuchten-Mualem (VGM) model (Mualem, 1976; van Genuchten, 1980). The shape parameters of α, n and θ_r were estimated using the Rosetta pedotransfer function (Schaap et al., 2001). Then SWC at field capacity was determined at a standard soil suction of 33 kPa. For further details on the estimation and calibration procedures of soil hydraulic parameters, please referred to Turkeltaub et al. (2018).

2.5.3. Eco-physiological parameters

Eco-physiological parameters for the three plants are summarized in Table 1 in which all values are derived from published data for *R. pseudoacacia*, *C. korshinskii* and *M. sativa* (Ding et al., 1996; Bai et al., 1999; Bai and Bao, 2002; Xu et al., 2001; Bon-Lamberty et al., 2005; Xia and Shao, 2008; Zheng and Shangguan, 2006; Song et al., 2013). The root distribution for the three plants was determined from the studies of Cheng et al. (2009) and Jian et al. (2014). The maximum root depth was assumed to be constant and equal to 500 cm for the three plants (Yang et al., 1994; Jia et al., 2017a).

2.6. Statistical analysis and accuracy evaluation of estimated AET

A set of statistical parameters (including mean, standard deviation, minimum and maximum values) was used to analyze simulated AET, LAI and NPP for each rainfall zone. Pearson correlation analysis was used to determine the relationships among AET, LAI, NPP with climate, soil texture and elevation for the three plants. A step-wise regression analysis was then used to select the main variables that accurately predict NPP for each species. All the statistical analyses were performed by

SPSS 15.0. Maps of the sampling sites and AET, LAI and NPP distributions were produced in GIS software (ArcGIS 9.2).

The performance of the modified Biome-BGC model was evaluated by statistical analyses. Simple liner regression analyses were used to calculate the coefficients of determination (R^2) between simulated and measured values. Mean difference (MD), root mean square error (RMSE) and mean absolute percent error (MAPE) were also used to evaluate the accuracy of AET estimation by the modified Biome-BGC model; which low values indicate high accuracy. The indices were calculated as follows:

$$MD = \frac{\sum_{i=1}^{n}(\hat{Z}_i - Z_i)}{n} \quad (2)$$

$$RMSE = \sqrt{\frac{1}{n}\sum_{i=1}^{n}(Z_i - \hat{Z}_i)^2} \quad (3)$$

$$MAPE = \frac{1}{n}\sum_{i=1}^{n}\left|\frac{\hat{Z}_i - Z_i}{Z_i}\right| \times 100 \quad (4)$$

where Z_i and $\hat{Z}_i$ are the measured and simulated values of AET, respectively for the *i*th observation; and *n* is the number of observations.

3. Results

3.1. Model evaluation

The model performance was examined by linearly regressing the simulated AET and the corresponding field measurement (Fig. 4). The simulated and observed AET generally agreed well for the three plant species with R^2 of 0.76, 0.80 and 0.91 for *R. pseudoacacia*, *C. korshinskii* and *M. sativa*, respectively. The model was again evaluated by MD, RMSE and MAPE analysis with respective values of –9.49 mm, 51.08 mm and 9.54% for *R. pseudoacacia*, –19.89 mm, 59.76 mm and 15.62% for *C.*

korshinskii and –17.62 mm, 52.20 mm and 10.50% for *M. sativa* (Table 2). Based on the statistical measures for the simulated and observed AET, the model performance was better for *R. pseudoacacia* than *C. korshinskii* and *M. sativa*. The above results indicated that the performance of the modified Biome-BGC model in terms of simulating AET dynamics was well acceptable for the three plant species. Thus, it was considered suitable for simulating NPP and LAI for the three dominant tree, shrub and grass species in the study area.

3.2. Spatial distribution of AET

AET for 1961–2014 was simulated using the modified Biome-BGC model driven by data from 243 sites across the China's LP study area. Based on the mean AET values for the 243 data sites, the spatial distributions of AET for the three species were mapped by kriging interpolation (Fig. 5). The ranges of the estimated AET were 287.7–619.5 mm for *R. pseudoacacia*, 287.8–617.7 mm for *C. korshinskii* and 312.5–619.6 mm for *M. sativa*, and with respective means of 464.7, 462.5 and 464.6 mm. The spatial distributions of AET for the three plant species were heterogeneous. AET generally increased from the northwest to the southeast, much the same as precipitation gradient. The three rainfall zones with MAP less than 450 mm, equal to 450–550 mm and above 550 mm had different AET values for each of the plant species (Table 3). For *R. pseudoacacia*, the >550 mm zone had the highest AET (554.0 mm) and the <450 mm zone the lowest AET (384.6 mm). AET for the 450–550 mm precipitation zone was 473.0 mm. Both *C. korshinskii* and *M. sativa* had similar spatial characteristics as *R. pseudoacacia* in terms of AET.

3.3. Spatial distribution of LAI and optimal plant cover

Based on mean maximum LAI for 1961–2014 from the 243 data sites in the study area, the spatial distribution of LAI for each plant species was derived by kriging interpolation (Fig. 6). The optimal plant cover was expressed as the mean maximum LAI of each plant. Consistent with the distribution of MAP, the optimal plant cover generally decreased from the southeast to the northwest, with ranges of 1.1–3.5 for *R. pseudoacacia*, 1.0–2.4 for *C. korshinskii* and 0.7–3.0 for *M. sativa* and corresponding means of 2.6, 1.8 and 1.3. The mean maximum LAI varied with rainfall zones (Table 3). It was 3.1 for the >550 mm precipitation zone, 2.7 for the 450–550 mm precipitation zone and 2.0 for the <450 mm precipitation zone under *R. pseudoacacia*. For *C. korshinskii*, it was 2.1 for the >550 mm precipitation zone, 1.9 for the 450–550 mm precipitation zone and 1.4 for the <450 mm precipitation zone. Then for *M. sativa* mean maximum LAI was 2.0, 1.2 and 0.9 for the three respective precipitation zones. The maximum LAI of *R. pseudoacacia* was always greater than that of *C. korshinskii* and *M. sativa* in any precipitation zone. Furthermore, the maximum LAI of *C. korshinskii* was much higher than that of *M. sativa* in both the 450–550 and the <450 mm precipitation zones. However, there was no significant difference in maximum LAI between *C. korshinskii* and *M. sativa* for the >550 mm precipitation zone (Table 3).

3.4. Spatial distribution of NPP and optimal SWCCV

Mean NPP was simulated for the three plant species using data from 243 sites across the plateau, and the spatial distribution of mean NPP for each plant species was mapped by kriging interpolation (Fig. 7). The mean NPP was considered as the optimal SWCCV. Consistent with mean AET and mean maximum LAI, the optimal SWCCV decreased from the southeast to the northwest of the study area. The respective ranges were 202.4–616.5 g C m^{-2} $year^{-1}$ for *R. pseudoacacia*, 83.7–201.7 g C m^{-2} yr^{-1} for *C. korshinskii* and 56.3–253.0 g C m^{-2} yr^{-1} for *M. sativa*. The overall mean NPP was 460.4 g C m^{-2} $year^{-1}$ for *R. pseudoacacia*, 152.2 g C m^{-2} yr^{-1} for *C. korshinskii* and 109.6 g C m^{-2} yr^{-1} for *M. sativa*. The highest mean NPP was for the >550 mm precipitation zone — 551.3, 181.7 and 165.8 g C m^{-2} yr^{-1} respectively for *R. pseudoacacia*, *C. korshinskii* and *M. sativa.* The mean NPP for the 450–550 mm precipitation zone was 489.1, 158.7 and 100.5 g C m^{-2} yr^{-1} respectively for *R. pseudoacacia*, *C. korshinskii* and *M. sativa*. The lowest mean NPP was for the <450 mm precipitation zone and it was 357.4, 121.6 and 74.5 g C m^{-2} yr^{-1} for *R. pseudoacacia*, *C. korshinskii* and *M. sativa*, respectively (Table 3).

3.5. Mean AET, LAI and NPP distribution factors

There was a highly significant positive relationship between mean AET and MAP for each plant species (n = 243, p < 0.001) (Table 4), suggesting that MAP was a major determinant of the spatial distribution of mean AET in China's LP region. Furthermore, the mean AET was significantly positively correlated with mean annual temperature (MAT), clay and silt contents. It was negatively correlated with elevation and sand content (n = 243, p < 0.001). Similar to AET, both the maximum LAI and mean NPP were significantly positively correlated with MAP, MAT, clay and silt contents, but negatively correlated with elevation and sand content for all the three plant species (n = 243, p < 0.001).

A step-wise regression analysis (significant at p < 0.001) was used to determine the main climatic and soil variables that accurately predict the regional spatial distribution of mean NPP for each plant species (Table 5). For *R. pseudoacacia*, 89.5% of the spatial variation in mean NPP was explained by MAP, MAT, clay content and elevation. Some 85.5 of the spatial variation in mean NPP for *C. korshinskii* and 91.3% of it for *M. sativa* were explained by MAP, MAT, silt content and elevation. Because of the strong correlation between NPP and LAI, the main contributing factors to the spatial distribution of mean maximum LAI were similar to those of mean NPP for each plant species. This suggested that the regional spatial distribution of optimal land cover or SWCCV for non-native tree, shrub and grass species in the study area was controlled by climate, soil and elevation.

4. Discussions

4.1. Spatial variations of AET and the driving factors

By comparison of simulated with observed AET, it was demonstrated that the modified Biome-BGC model can simulate temporal dynamics of evapotranspiration for *R. pseudoacacia*, *C. korshinskii* and *M. sativa* in the study area. Considering the strong correlations among AET, NPP and LAI (Fassnacht and Gower, 1997; Schimel et al., 1997; Bond-Lamberty et al., 2009; Feng et al., 2012), the modified Biome-BGC model could be used to determine NPP and LAI of the three plant species. It is important to note that the simulated AET was much lower than the observed one for high values (Fig. 4). This suggested that errors existed in the method (i.e., the water balance approach) used to measure AET. The measured AET was derived from SWC in the 0–500 cm soil profile measured at the start and end of the growing season. High AET was mostly in wet years during which time there was enhanced flow of water from shallow to deep soil layers. The instantaneous measurements of SWC in the 0–500 cm soil layer at the start and end of the growing season could have overestimated AET due to the possible inclusion of percolations during wet periods and therefore the high observed AET. Furthermore, many eco-physiological parameters of the three plant species used as model input varied with rainfall and temperature in the Loess Plateau study area (Zheng and Shangguan, 2006, 2007). Ignoring spatial variations in eco-physiological parameters of each plant species due to differences in climatic and soil conditions (White et al., 2000) could also have resulted in the inaccurate estimation of AET. Nevertheless, based on the three statistics (MD, RMSE and MAPE) of the simulated and observed AET, the Biome-BGC model proved to be a useful tool for analyzing the climate-soil-vegetation relationship in semi-arid, sub-humid regions.

Studies show that the distribution pattern of AET is driven by various environmental factors, including precipitation, temperature, solar radiation, relative humidity and vegetation density (e.g. NDVI or LAI) (Nosetto et al., 2005; Wang et al., 2010; Shi et al., 2013). For example, the variability of evapotranspiration in China during the period 1982–2015 was significantly correlated with temperature, solar radiation and relative humidity, indicating how critical surface meteorological conditions were for evapotranspiration (Li et al., 2018). In this study, the spatial pattern of mean AET notably decreased from the southeast to the northwest, much the same as annual precipitation (Fig. 5). The range of Pearson correlation coefficient between AET and MAP was 0.978–0.999, indicating the impactful contribution of MAP to AET variability in the study area. Thus, the long-term mean AET was almost equal to MAP in the plateau study area (Yang et al., 1994). Although a significant positive correlation existed between mean AET and MAT, the correlation coefficient was much lower than that with MAP (Table 4). This is in agreement with the findings of Liu et al. (2016) that precipitation mainly controlled the spatio-temporal variations in ET in arid and semi-arid areas of China. This variation was attributed to the limited precipitation as the sole source of soil water because groundwater levels in the semi-arid plateau region were generally 30–100 m below the land surface, far beyond rooting depth (Jia et al., 2017a; Zhu et al., 2018). The mean AET was negatively correlated with elevation and sand content, but positively correlated with clay and silt contents. High elevation corresponds to low MAT and then low AET in the study area. Coarse soil texture has low water holding capacity, high drainage loss and low available soil water, and hence low AET. Low nutrient associated with low water holding capacity of coarse soils can also limit AET by retarding plant growth. This is consistent with the finding that soil texture strongly influences AET (Hillel, 1998; Nosetto et al., 2005).

4.2. Optimal SWCCV and the driving variables

Since the early 1950s, re-vegetation has been the main mode of control of soil erosion and other forms of land degradation in China's LP. The significant increase in vegetation cover has enhanced soil conservation (Lü et al., 2012; Wang et al., 2016), carbon sequestration (Deng et al., 2014) and bio-conservation (Jia et al., 2011) in the semi-arid LP. It, however, has also increased soil water loss via evapotranspiration (particularly of exotic plant species and high density planting fields), causing imbalances in soil water availability and utilization for plant growth. The excessive re-vegetation has not only decreased regional water yield (Lü et al., 2012), but also intensified deep soil water depletion (Jia et al., 2017a) in the region, leading to the formation of dry soil layers. This has in turn threatened the health and sustainability of the ecosystem due to lack of available water resources. Excessive re-vegetation using *C. korshinskii* has caused severe soil water deficit after 10 years of growth and dry soil layers have developed to the depth of 1–9 m (Li et al., 2007). Jia et al. (2017b) showed that mean loss of soil water in the 1–5 m profile due to the conversion of agricultural lands to forest across China's LP was ~204 mm, occurring at the rate of 16.2 mm yr^{-1}. Also once a dry soil layer is formed; it is difficult to reclaim any such land in the plateau study area due to limited rainfall, deep water table, high water use by vegetation and intense evaporation. According to Liu et al. (2010), it could require

~18 years to restore the 0–6 m SWC of alfalfa grassland to cropland conditions in mountain regions of southern Ningxia.

Reports of the problems of soil desiccation due to excessive re-vegetation have become common placed in the last few years. This issue should be addressed if the replanting effort is to result in optimal vegetation cover under the given climatic and edaphic conditions. The study indicated that the ranges of optimal plant cover in the study area were 1.1–3.5 for *R. pseudoacacia*, 1.0–2.4 for *C. korshinskii* and 0.7–3.0 for *M. sativa*. Then those for optimal NPP were 202.4–616.5 g C m^{-2} yr^{-1} for *R. pseudoacacia*, 83.7–201.7 g C m^{-2} yr^{-1} for *C. korshinskii* and 56.3–253.0 g C m^{-2} yr^{-1} for *M. sativa*; with corresponding means of 460.4, 152.2 and 109.6 g C m^{-2} yr^{-1}. The simulated values for *R. pseudoacacia* were consistent with those given by Sun and Zhu (2000), with NPP of 459.7 g C m^{-2} yr^{-1} for deciduous broad-leaf forests on China's LP. Using a mathematical model, Zhang et al. (2003) noted simulated NPP of 466 g C m^{-2} yr^{-1} for deciduous broad-leaf forests in northern China.

For comparison with other studies, the factor 0.46 and 0.40 were used to convert NPP (i.e., biomass carbon) to dry biomass production for *C. korshinskii* and *M. sativa*, respectively. The spatial distribution of mean dry biomass for both plants is shown in Fig. S1. The ranges of the optimal dry biomass for *C. korshinskii* and *M. sativa* were 1.9–4.5 and 1.4–6.3 t ha^{-1} yr^{-1}, with mean values of 3.4 and 2.7 t ha^{-1} yr^{-1}, respectively. The biomass for *C. korshinskii* (3.0 t ha^{-1} yr^{-1}) and *M. sativa* (1.9 t ha^{-1} yr^{-1}) in this study was different from those reported by Xia and Shao (2008), which was 3.4 and 1.6 t ha^{-1} yr^{-1} for *C. korshinskii* and *M. sativa*, respectively for the Liudaogou catchment in China's northern LP region. The optimal plant cover corresponded with maximum LAI (1.3) for *C. korshinskii* simulated using the SHAW model (Fu et al., 2012), for which it was also different from that (1.6) obtained in our study. The inconsistent results could be due to the differences in climate during the study periods. The study period for the earlier studies was only 2–3 years, which could not sufficiently represent long-term variability of SWCCV due to large fluctuations in precipitation in the study area. Annual and inter-annual variations in precipitation can be very widely between dry and wet years. Our study considered the variations in the long-term climatic conditions by covering the entire period of 1961–2014 in simulating NPP and LAI for the three plant species. The optimal NPP and maximum LAI were thus more representative of the long-term variability of SWCCV in the study area.

The optimal plant cover and SWCCV for each plant species generally decreased from the southeast to the northwest, following the precipitation gradient. Step-wise regression analysis indicated that MAP, MAT, elevation and soil texture were the main factors contributing to NPP for the three plant species in the study area, with more than 86% of the spatial variation in mean NPP explained by these variables (Table 5). Precipitation, a proxy for water availability, is reported to be the key factor controlling annual NPP in most terrestrial ecosystems in the world, especially in arid and semi-arid regions (Knapp and Smith, 2001; Zhang et al., 2015a). As a key determinant of water/nutrient storage and transport, soil texture has a strong influence on the growth of plants. Silt with main texture variable contributing to NPP of both *C.*

korshinskii and *M. sativa*, implying that the growth of both plants favored medium-textured soils in the study area. This is because medium-textured soil offers the highest available water for plant growth as it well suited for a good balance low water holding capacity and high drainage loss of coarse-textured soils and poor infiltration, high moisture retention and runoff of fine-textured soils (Nosetto et al., 2005; Fensham et al., 2015). Soil water (matric) potential becomes much more negative on fine-textured soils than on coarse-textured soils when moisture content is low, implying that water in drying clay soils is more difficult for plants to extract than in drying sandy soils (Sperry and Hacke, 2002; Fensham et al., 2015). Clay, however, was the main texture driving NPP of *R. pseudoacacia*; ascribed to the high root water uptake ability of *R. pseudoacacia* than of *C. korshinskii* and *M. sativa* (Yan et al., 2017). Furthermore, the spatial variation in mean NPP was also highly dependent on elevation for all the three plant species since it modulated climate and/or water availability in the study area. This was in agreement with the reports of Camarero et al. (2013) and Sánchez-Salguero et al. (2015), implying that topographic features were necessary considerations in estimating NPP in China's LP. The relationship of mean maximum LAI to various other variables was similar to that of mean NPP for all the three plant species in the study area. The above results suggested that MAP, MAT, elevation and soil texture can be used to accurately estimate NPP and maximum LAI of all three plant species in the semi-arid plateau study area.

4.3. Implications for re-vegetation and land management

Increasing vegetation cover through re-vegetation is an effective measure for soil conservation. However, excessive re-vegetation can aggravate soil water scarcity and cause the formation of dry soil layers in the soil profile, which can in turn threaten the health and services of restored ecosystems. A balance between soil water availability and water utilization by plants is critical for maintaining ecosystem health in arid and semi-arid regions of China's LP. Therefore, an optimal plant cover not only controls soil erosion, but also maintains regional water balance and vegetation sustainability. As the most common tree, shrub and grass species in the restoration program in the LP, the spatial distributions of optimal plant cover and SWCCV for *R. pseudoacacia*, *C. korshinskii* and *M. sativa* were determined for different rainfall zones in the study area. This indicated that re-vegetation with non-native plants should consider vegetation thresholds of the various plant species to guide future re-vegetation drives. The current vegetation cover or NPP in many parts of the study area was already close to or even exceeded the climate-defined equilibrium vegetation cover (Feng et al., 2016; Zhang et al., 2018). The region is known for "small old trees" that grow only *ca* 20% of their normal height, indicating that the soil water consumption has exceeded SWCCV (Jia et al., 2017a). Management such as thinning or land-use change is required in overplanting areas to maintain a balance between soil water availability and plant use of available soil water. *M. sativa*, one of the most important forage crops in the world, is the most widely promoted species for artificial grasslands in the LP due to its high nutritive value, drought resistance and high adaptability to rigorous climatic and poor edaphic conditions (Cui et al., 2018). Local farmers can use the provided information on SWCCV to manage *M. sativa* grasslands in the region. China's LP is a water-limited region with precipitation as the main source of soil water. Thus, annual precipitation is an important factor for determining SWCCV, planting sites and densities. However, annual precipitation in the plateau region has been decreasing with increasing air temperature (Wang et al., 2011); increasing the challenge for future re-vegetation activities in the region. The quantification of optimal SWCCV for various plant species under future climate scenarios in the region is needed to guide future re-vegetation activities. Furthermore, this study indicated that soil texture and elevation were significantly correlated with SWCCV. Thus, because of the strong spatial variability of soil and topographic features in the region, future re-vegetation activities should consider soil texture and elevation with the highest potential to moderate site water and heat conditions.

5. Conclusions

To address the SWCCV in China's LP (where there is a large-scale re-vegetation project aimed at controlling soil erosion and restoring the natural ecological environment), AET, NPP and LAI dynamics for *R. pseudoacacia*, *C. korshinskii* and *M. sativa* were simulated with using modified Biome-BGC model. The results showed that the model accurately simulated AET for the three plant species in the region, suggesting that it can fairly simulate plant growth as AET and NPP are closely related linearly. The simulated AET, NPP and LAI generally decreased from the southeast to the northwest, following the precipitation gradient. Optimal plant cover in the study area (derived from maximum LAI) was 1.1–3.5 for *R. pseudoacaia*, 1.0–2.4 for *C. korshinskii* and 0.7–3.0 for *M. sativa*; corresponding to SWCCV (derived from NPP) values of 202.4–616.5, 83.7–201.7 and 56.3–253.0 g C m^{-2} yr^{-1}, respectively. Precipitation, temperature, elevation and soil texture were the main factors driving spatial variations in NPP and LAI of the three plant species. A re-vegetation threshold was recommended for the promotion of sustainable eco-hydrological environment in the region. Thus, future re-vegetation activities should consider climatic conditions, soil texture and topographic features to avoid the formation of dry soil layers after re-vegetation.

Acknowledgements

This study was supported by the National Key Research and Development Program of China (2016YFC0501605), the National Natural Science Foundation of China (41530854 and 41390461), the Youth Innovation Promotion Association of Chinese Academy of Sciences (2017076), the UK Natural Environment Research Council (NE/N007409/1) and the Youth Innovation Research Team Project (LENOM2016Q0001). We are indebted to the editors and reviewers for the insightful contributions by way of constructive comments and suggestions on the work. We acknowledge the invaluable inputs of Dr. Z. Liu, Dr. C. Zhao, Dr. L. Duan and Dr. C. Zhang in terms of data collection and critical suggestions.

References

Bai, W.M., Bao, X.M., 2002. Simulation alfalfa growth in Wulanbuhe sandy region. Chin. J. Appl. Ecol. 13(12), 1605-1609 (in Chinese).

Bai, Y.L., Wu, Y.H., Han, X.H., 1999. Study on the relationship between the plant age and the nutrient component of alfalfa. Pratacult. Sci. 16(1), 18-21 (in Chinese).

Bond-Lamberty, B., Gower, S.T., Ahl, D.E., Thornton, P.E., 2005. Reimplementation of the BIOME-BGC model to simulate successional change. Tree Physiol. 25, 413-424.

Bond-Lamberty, B., Peckham, S., Gower, D., Stith, T., 2009. Effects of fire on regional evapotranspiration in the central Canadian boreal forest. Global Change Biol. 15, 1242-1254.

Camarero, J.J., Manzanedo, R.D., Sánchez-Salguero, R., Navarro-Cerrillo, R., 2013. Growth response to climate and drought change along an aridity gradient in the southernmost *Pinus nigra* relict forests. Ann. For. Sci. 70, 769-780.

Chen, Y.P., Wang, K.B., Lin, Y.S., Shi, W.Y., Song, Y., He, X.H., 2015. Balancing green and grain trade. Nat. Geosci. 8, 739-741.

Cheng, J., Wan, H., 2002. Vegetation Constructions and Water Constructions and Water Conservation in the Loess Plateau in China. Chinese Forestry Publishing Press, Beijing, pp. 208-340 (in Chinese)

Cheng, X., Huang, M., Shao, M., Warrington, D.N., 2009. A comparison of fine roots distribution and water consumption of mature *Caragana korshinkii* Kom grown in two soils of the semiarid region, China. Plant Soil 315, 149-161.

Chirino, E., Bonet, A., Bellot, J., Sanchez, J.R., 2006. Effects of 30-year-old Aleppo pine plantations on runoff, soil erosion, and plant diversity in a semi-arid landscape in south eastern Spain. Catena 65, 19-29.

Cong, Z., Li, Q., Mo, K., Zhang, L., Shen, H., 2017. Ecohydrological optimality in the Northeast China Transect. Hydrol. Earth Syst. Sci. 21, 2449-2462.

Cui, Z., Liu, Y., Jia, C., Huang, Z., He, H.H., Han, F.P., Shen, W.B., Wu, G.L., 2018. Soil water storage compensation potential of herbaceous energy crops in semi-arid region. Field Crop. Res. 223, 41-47.

Deng, L., Liu, G.B., Shangguan, Z.P., 2014. Land-use conversion and changing soil carbon stocks in China's 'Grain-for-Green' Program: a synthesis. Global Change Biol. 20 (11), 3544-3556.

Ding, L., Zhong, Z.P., Li, S.Y., Zhang, C.H., Bai, K.Z., Kuang, T.Y., 1996. Assimilation and allocation of carbon and nitrogen in alfalfa under doubled CO_2 environment. Acta Bot. Sin. 38(1), 83-86 (in Chinese).

Eagleson, P.S., 2002. Ecohydrology: Darwinian expression of vegetation form and function, Cambridge University Press, Cambridge.

Eaton, J.M., MvGoff, N.M., Byme, K.A., Leahy, P., Kiely, G., 2008. Land cover change and soil organic carbon stocks in the Republic of Ireland 1851-2000. Climatic Change 91, 317-334.

Farquhar, G.D., von Caemmerer, S., Berry, J.A., 1980. A biochemical model of photosynthetic CO_2 assimilation in leaves of C_3 species. Planta 149, 78-90.

Fassnacht, K.S., Gower, S.T., 1997. Interrelationships among the edaphic and stand characteristics leaf area index, and aboveground net primary production of upland forest ecosystems in north central Wisconsin. Can. J Forest Res. 27, 1058-1067.

Fensham, R.J., Butler, D.W., Foley, J., 2015. How does clay constrain woody biomass in drylands? Global Ecol. Biogeogr. 24, 950-958.

Feng, X.M., Sun, G., Fu, B.J., Su, C.H., Liu, Y., Lamparski, H., 2012. Regional effects of vegetation restoration on water yield across the Loess Plateau, China. Hydrol. Earth Syst. Sci. 16, 2617-2628.

Feng, X.M., Fu, B.J., Piao, S.L., Wang, S., Ciais, P., Zeng, Z.Z., et al., 2016. Revegetation in China's Loess Plateau is approaching sustainable water resource limits. Nat. Clim. Chang. 6:1019-1022.

Fu, W., Huang, M.B., Gallichand, J., Shao, M.A., 2012. Optimization of plant coverage in relation to water balance in the Loess Plateau of China. Geoderma 173-174, 134-144.

Guo, Z.S., Shao, M.A., 2004. Mathematical model for determining vegetation carrying capacity of soil water. J. Hydraul. Eng. 10, 95-99 (in Chinese).

Hartkamp, A.D., Beurs, K.D., Stein, A., White, J.W., 1999. Interpolation Techniques for Climate Variables. NRG-GIS Series 99-01. CIMMYT, Mexico, DF.

Hillel, D., 1998. Environmental Soil Physics. Academic Press, San Diego.

Huang, M.B., Zettl, J.D., Barbour, S.L., Elshorbagy, A., Si, B.C., 2013. The impact of soil moisture availability on forest growth indices for variably layered coarse-textured soils. Ecohydrology 6, 214-227.

Jia, X.X., Shao, M.A., Wei, X.R., 2011. Richness and composition of herbaceous species in restored shrubland and grassland ecosystems in the northern Loess Plateau of China. Biodivers. Conserv. 20(4), 3435-3452.

Jia, X.X., Shao, M.A., Zhu, Y.J., Luo, Y., 2017a. Soil moisture decline due to afforestation across the Loess Plateau, China. J Hydrol. 546, 113-122.

Jia, X.X., Wang, Y.Q., Shao, M.A., Luo, Y., Zhang, C.C., 2017b. Estimating regional losses of soil water due to the conversion of agricultural land to forest in China's Loess Plateau. Ecohydrology 10(6), e1851.

Jian, S.Q., Zhao, C.Y., Fang, S.M., Yu, K., 2014. Distribution of fine root biomass of main planting tree species in Loess Plateau, China. Chin. J. Appl. Ecol. 25(7), 1905-1911 (in Chinese).

Jian, S.Q., Zhao, C.Y., Fang, S.M., Yu, K., 2015. Effects of different vegetation restoration on soil water storage and water balance in the Chinese Loess Plateau. Agr. Forest Meteorol. 206, 85-96.

Klute, A., Dirksen, C., 1986. Hydraulic conductivity of saturated soils. In: Klute, A. (Ed.), Methods of Soil Analysis. ASA and SSSA, Madison, Wisconsin, USA, pp. 694-700.

Knapp, A.K., Smith, M.D., 2001. Variation among biomes in temporal dynamics of aboveground primary production. Science 291, 481-484.

Li, H.J., Wang, M.B., Chen, L.F., Cai, B.F., 1996. Study on hydrologic ecology of *Robinia pseudoacacia* population in northwestern Shanxi. Acta Ecol. Sin. 20, 151-158 (in Chinese).

Li, X.F., Li, J., Wang, X.C., Zhao, Y.J., Cheng, J.M., Shao, M.A., 2007. Simulation of water productivity and soil desiccation of Caragana microphylla shrub land on semi-arid hilly region of the Loess Plateau. Agr. Res. Arid Areas 25, 113-120. (in Chinese).

Li, R., Yang, W.Z., Li, B.C., 2008. Research and future prospects for the Loess Plateau of China. Beijing: Science press (in Chinese).

Li, Y.S., Huang, M.B., 2008. Pasture yield and soil water depletion of continuous growing alfalfa in the Loess Plateau of China. Agr. Ecosyst. Environ. 124, 24-32.

Li, X., He, Y., Zeng, Z., Lian, X., Wang, X., Du, M., Jia, G., Li, Y., Ma, Y., Tang, Y., Wang, W., Wu, Z., Yan, J., Yao, Y., Ciais, P., Zhang, X., Zhang, Y., Zhang, Y., Zhou, G., Piao, S., 2018. Spatiotemporal pattern of terrestrial evapotranspiration in China during the past thirty years. Agr. Forest Meteorol. 259, 131-140.

Liu, Z., Tim, R., Li, L., Tom, G., Yan, Q., Li, R., Mu, X., 2008. Interpolation for time series of meteorological variables using ANUSPLIN. J Northwest A F Univ. (Nat. Sci. Ed.), 36(10), 227-234 (in Chinese).

Liu, P.S., Z.K. Jia, J. Li, J.P. Wang, Q.F. Han. 2010. Effects of different alfalfa-crop rotation patterns on water recovery of degradation alfalfa grassland. Trans. Chin. Soc. Agric. Eng. 26(2), 95-102. (In Chinese).

Liu, B., Shao, M., 2015. Modeling soil-water dynamics and soil-water carrying capacity for vegetation on the Loess Plateau, China. Agr. Water Manage. 159, 176-184.

Liu, J.G., Jia, B.H., Xie, Z.H., Shi, C.X., 2016. Ensemble simulation of land evapotranspiration in China based on a multi-forcing and multi-model approach. Adv. Atmos. Sci. 33, 673-684.

Lü, Y., Fu, B., Feng, X., Zeng, Y., Liu, Y., Chang, R., Sun, G., Wu, B., 2012. A Policy-Driven Large Scale Ecological Restoration: Quantifying Ecosystem Services Changes in the Loess Plateau of China. PLoS ONE 7(2): e31782.

McVicar, T.R., van Niel, T.G., Li, L., Wen, Z., Yang, Q., Li, R., Jiao, F., 2010. Parsimoniously modelling perennial vegetation suitability and identifying priority areas to support China's re-vegetation program in the Loess Plateau: Matching model complexity to data availability. Forest Ecol. Manag. 259, 1277-1290.

Mo, K., Cong, Z., Lei, H., 2016. Optimal vegetation cover in the Horqin Sands, China. Ecohydrology 9, 700-711.

Mualem, Y., 1976. A new model for predicting the hydraulic conductivity of unsaturated porous media. Water Resour. Res. 12, 513-522.

Nosetto, M.D., Jobbágy, E.G., Paruelo, J.M., 2005. Land-use change and water losses: the case of grassland afforestation across a soil textural gradient in central Argentina. Global Change Biol. 11, 1101-1117.

Palmroth, S., Katul, G.G., Hui, D., McCarthy, H.R., Jackson, R.B., Oren, R., 2010. Estimation of long-term basin scale evapotranspiration from streamflow time series, Water Resour. Res. 46, W10512.

Sánchez-Salguero, Camarero, J.J., Hevia, A., Madrigal-González, J., Linares, J.C., Ballesteros-Canovas, J.A., Sánchez-Miranda, A., Alfaro-Sánchez, R., Sangüesa-Barreda, G., Galván, J.D., Gutiérrez, E., Génova, M., Rigling, A., 2015. Agr. Forest Meteorol. 206, 151-162.

Schaap, M.G., Leij, F.J., van Genuchten, M.T., 2001. ROSETTA: A computer program for estimating soil hydraulic parameters with hierarchical pedotransfer functions. J Hydrol. 251, 163-176.

Schimel, D.S., Braswell, B.H., Parton, W.J., 1997. Equilibration of the terrestrial water, nitrogen, and carbon cycles. Proc. Natl. Acad. Sci. U. S. A. 94, 8280-8283.

Shi, H., Shao, M., 2000. Soil and water loss from the Loess Plateau in China. J Arid Environ. 45, 9-20.

Shi, X., Mao, J., Thornton, P.E., et al., 2013. Spatiotemporal patterns of evapotranspiration in response to multiple environmental factors simulated by the community land model. Environ. Res. Lett. 8, 24012.

Shao, M., Wang, Y., Xia, Y., Jia, X., 2018. Soil drought and water carrying capacity for vegetation in the critical zone of the Loess Plateau: A review. Vadose Zone J. 17, 170077.

Song, G., Wen, Z., Zheng, Y., 2013. Relationships between plant functional traits of *Robinia Pseudoacacia* and meteorological factors in Loess Plateau, North Shaanxi, China. Res. Soil Water Conserv. 20, 125-130 (in Chinese).

Sperry, J.S., Hacke, U.G., 2002. Desert shrub water relations with respect to soil characteristics and plant functional type. Funct. Ecol. 16, 367-378.

Sun, R., Zhu, Q., 2000. Distribution and seasonal change of net primary productivity in China from April, 1992 to March, 1993. Acta Geogra. Sin. 55(1), 36-45 (in

Chinese).

Thornton, P.E., Hasenauers, H., White, M.A., 2000. Simultaneous estimation of daily solar radiation and humidity from observed temperature and precipitation: An application over complex terrain in Austria. Agr. Forest Meteorol. 104(4), 255-271.

Thornton, P.E., Law, B.E., Gholz, H.L., Clark, K.L., Falge, E., Ellsworth, D.S., Goldstein, A.H., Monson, R.K., Hollinger, D., Falk, M., Chen, J., Sparks, J.P., 2002. Modeling and measuring the effects of disturbance history and climate on carbon and water budgets in evergreen needleleaf forests. Agric. For. Meteorol. 113(1-4), 185-222.

Turkeltaub, T., Jia, X., Zhu, Y., Shao, M.A., Binley, A., 2018. Recharge and nitrate transport through the deep vadose zone of the Loess Plateau: a regional-scale model investigation. Water Resour. Res. 54, 4332-4346.

van Genuchten, M.T., 1980. A closed-form equation for predicting the hydraulic conductivity of unsaturated soils. Soil Sci. Soc. Am. J. 44, 892-898.

Wang, K., Dickinson, R.E., Wild, M., et al., 2010. Evidence for decadal variation in global terrestrial evapotranspiration between 1982 and 2002: 2. Results. J. Geophys. Res. Atmos. 115, D20113.

Wang, Y., Shao, M., Zhu, Y., Liu, Z.P., 2011. Impacts of land use and plant characteristics on dried soil layers in different climatic regions on the Loess Plateau of China. Agr. Forest Meteorol. 151, 437-448.

Wang, S., Fu, B.J., Piao, S.L., Lü, Y.H., Philippe, C., Feng, X.M., Wang, Y.F., 2016.

Reduced sediment transport in the Yellow River due to anthropogenic changes. Nat. Geosci. 9, 38-41.

White, M.A., Thornton, P.E., Running, S.W., Nemani, R.R., 2000. Parameterization and sensitivity analysis of the BIOME-BGC terrestrial ecosystem model: net primary production controls. Earth Interact. 4, 1-85.

Xia, Y.Q., Shao, M.A., 2008. Soil water carrying capacity for vegetation: A hydrologic and biogeochemical process model solution. Ecol. Model. 214, 112-124.

Xu, D.M., Cui, W.X., Guo, S.J., Sun, X.C., 2001. The dynamics of mutrient contents in several psammophyte shrubs in Maowusu sandland, Ningxia, China. Pratacult. Sci. 18(6), 23-26 (in Chinese).

Yan, W.M., Zhong, Y.Q.W., Shangguan, Z.P., 2017. Responses of different physiological parameter thresholds to soil water availability in four plant species during prolonged drought. Agr. Forest Meteorol. 247, 311-319.

Yang, X., Yang, W., 1989. A preliminary study on the soil water balance of artificial forestland in loess-hilly region. Scie. Silvae Sin. 25(6), 549-553 (in Chinese).

Yang, X., Yang, W., Ma, Y., 1994. Study on the condition growing of the man-made Locust Woodland and moisture eco-environment in the small watershed of Zhifanggou. Res. Soil Water Conserv. 1, 31-35 (in Chinese).

Yaseef, N.R., Yakir, D.E., Rotenberg, S.G., Cohen, S., 2009. Ecohydrology of a semi-arid forest: partitioning among water balance components and its implications for predicted precipitation changes. Ecohydrology 3, 143-154.

Zhang, N., Yu, G., Zhao, S., 2003. Ecosystem productivity process model for landscape based on remote sensing and surface data. Chin. J. Appl. Ecol. 14, 643-652 (in Chinese).

Zhang, Y., Huang, M.B., Lian, J.J., 2015a. Spatial distributions of optimal plant coverage for the dominant tree and shrub species along a precipitation gradient on the central Loess Plateau. Agr. Forest Meteorol. 206, 69-84.

Zhang, L.D., Zhang, Y., Huang, M.B., Zhu, Y.J., 2015b. Simulations of soil water balance in two Arbor forests grown in gully region of the Loess Plateau. Res. Soil Water Conserv. 22(2), 26-31 (in Chinese).

Zhang, S., Yang, D., Yang, Y., Piao, S., Yang, H., Lei, H., Fu, B., 2018. Excessive afforestation and soil drying on China's Loess Plateau. J. Geophys. Res-Biogeo. 123, 923-935.

Zhao, S., 2012. Evolution characteristics of soil organic carbon-structure-water environment under vegetation restoration on the Ziwuling Mountain, Loess Plateau. In:PhD Dissertation. Institute of Soil and Water Conservation, The Chinese Academy of Science, Yangling, Shaanxi Province, China (in Chinese).

Zhao, C., Shao, M., Jia, X., Nasir, M., Zhang, C., 2016. Using pedotransfer functions to estimate soil hydraulic conductivity in the Loess Plateau of China. Catena 143, 1-6.

Zheng, S.X., Shangguan, Z.P., 2006. The spatial distribution pattern of plant leaves nutrient composition in the Loess Plateau region. Prog. Nat. Sci. 16, 965-973 (in Chinese).

Zheng, S.X., Shangguan, Z.P., 2007. Spatial patterns of photosynthetic characteristics and leaf physical traits of plants in the Loess Plateau of China. Plant Ecol. 191, 279-293.

Zhu, Y.J., Jia, X.X., Shao, M.A., 2018. Loess thickness variations across the Loess Plateau of China. Surv. Geophys. 39, 715-727.

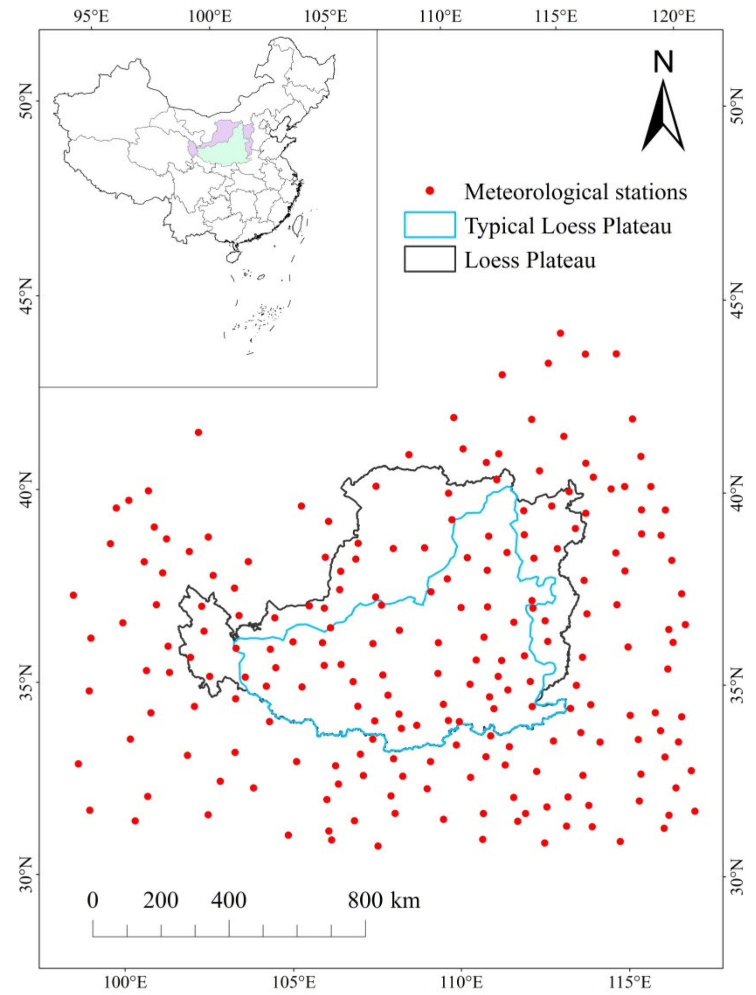

Fig. 1 A map depicting the location of the Loess Plateau in China (inset at top left corner) and an expanded map of the plateau (main plate) with red dots depicting the locations of the stations (213) for monitoring climate in and around the Loess Plateau.

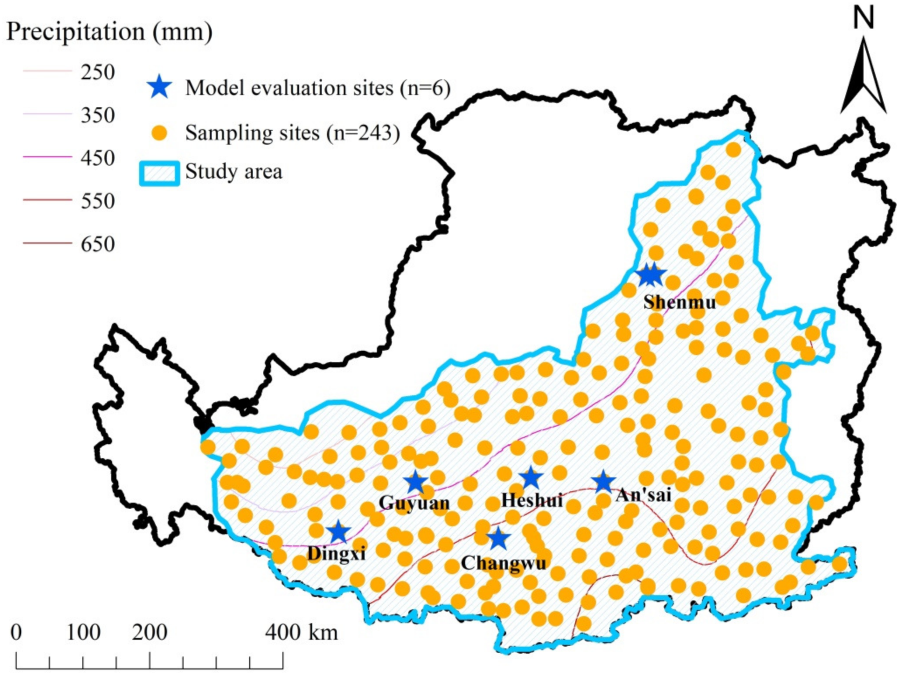

Fig. 2 A map depicting the location of the study area in the Loess Plateau and the distributions of the 243 sampling sites, six model evaluation sites and precipitation contours in the region.

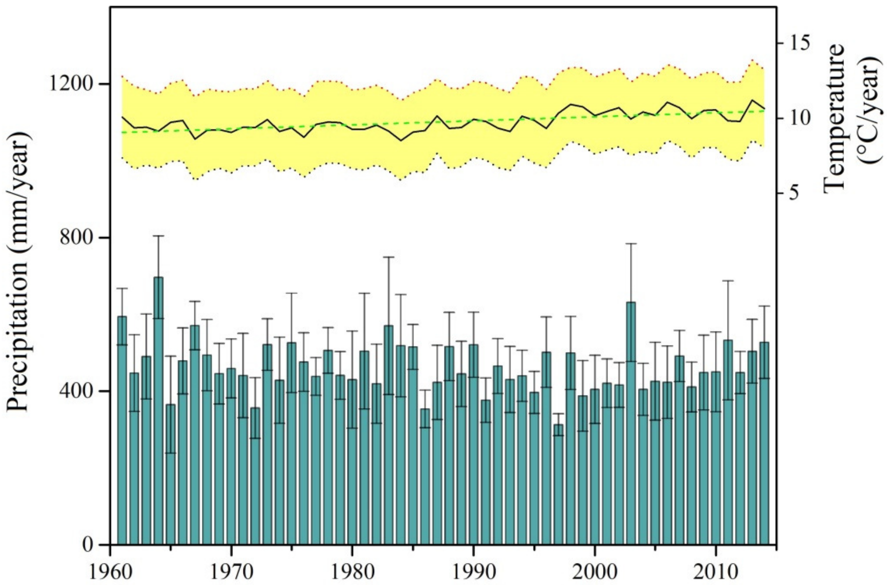

Fig. 3 Plot of average annual precipitation and air temperature in the Loess Plateau study area. The shaded area denotes the ±1.0 standard deviation range.

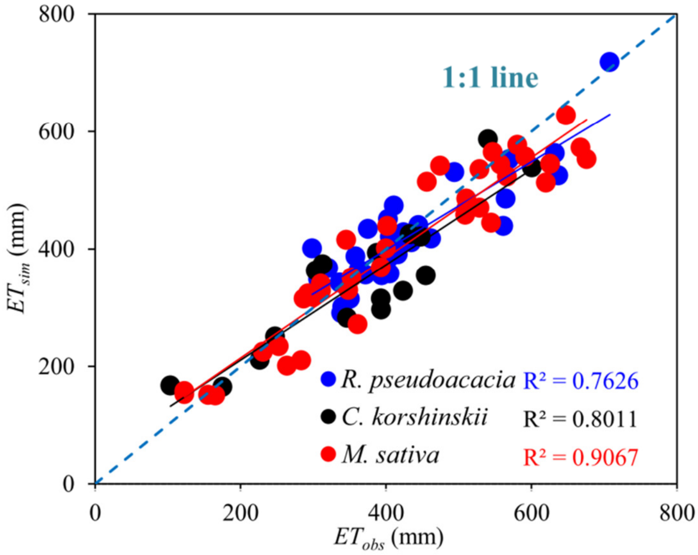

Fig. 4 A plot of comparison of simulated (ET_{sim}) versus observed (ET_{obs}) evapotranspiration for *Robinia pseudoacacia*, *Caragana korshinskii* and *Medicago sativa* at six sites in the Loess Plateau study area.

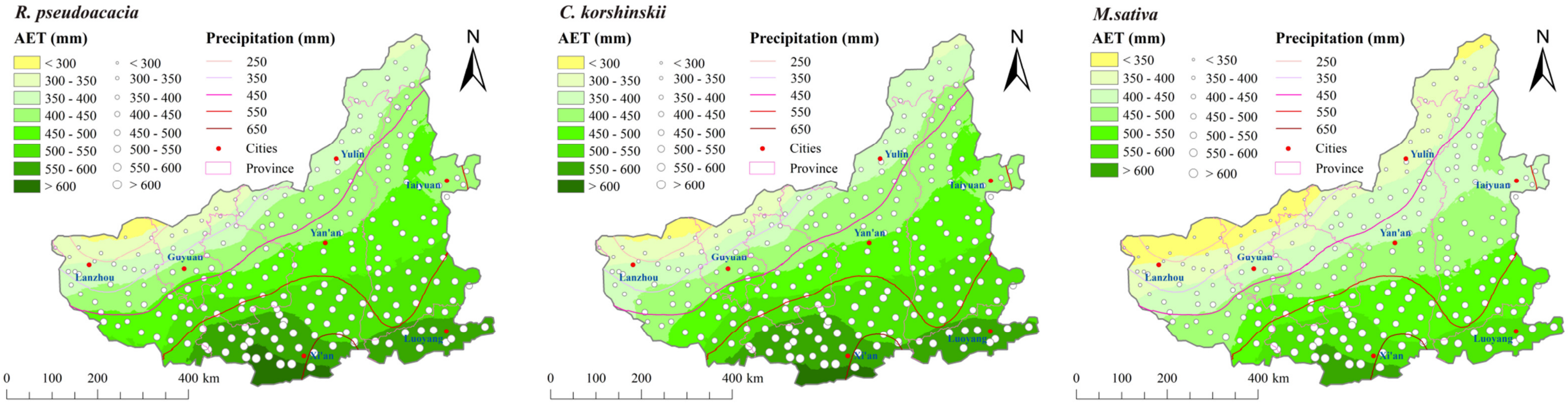

Fig. 5 Spatial distributions of mean actual evapotranspiration (AET) for *Robinia pseudoacacia*, *Caragana korshinskii* and *Medicago sativa* in the Loess Plateau study area.

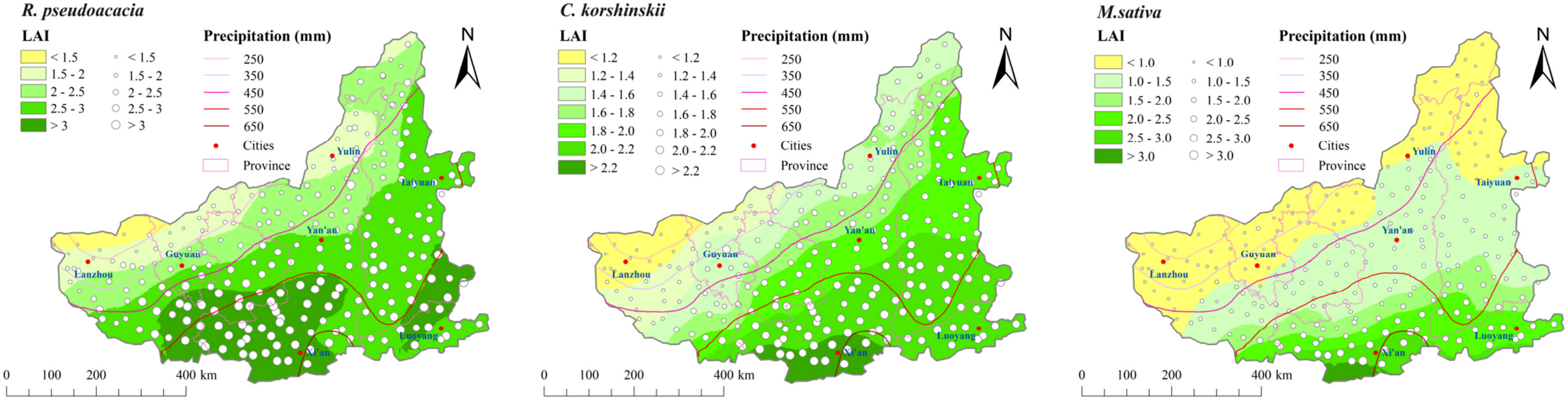

Fig. 6 Spatial distributions of mean maximum LAI for *Robinia pseudoacacia*, *Caragana korshinskii* and *Medicago sativa* in the Loess Plateau study area.

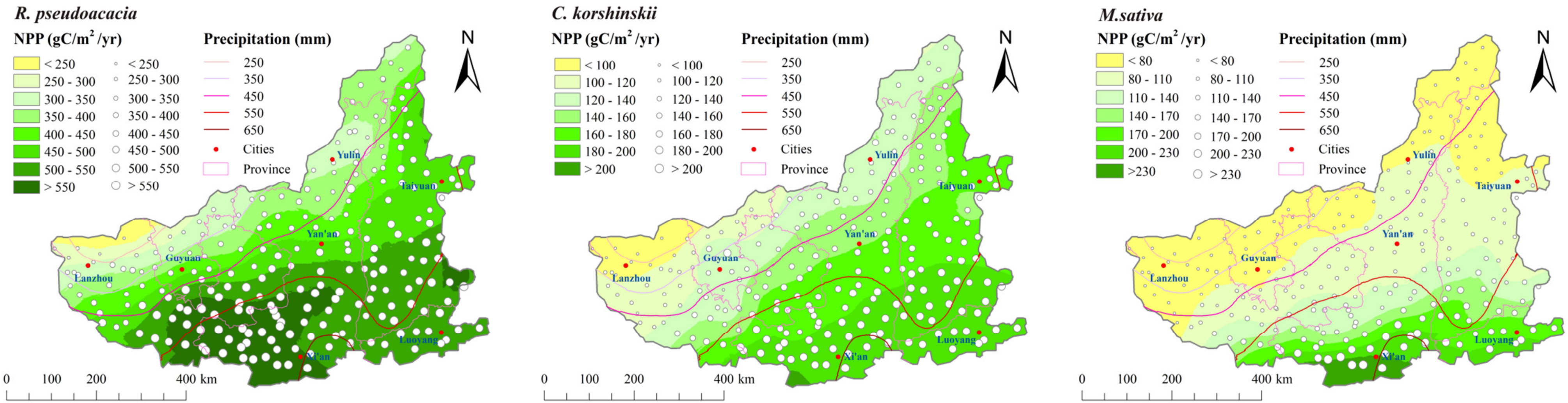

Fig. 7 Spatial distributions of mean net primary productivity (NPP) for *Robinia pseudoacacia*, *Caragana korshinskii* and *Medicago sativa* in the Loess Plateau study area.

Table 1 Eco-physiological parameters for *Robinia pseudoacacia*, *Caragana korshinskii* and *Medicago sativa*.

Parameter	*R. pseudoacacia*	*C. korshinskii*	*M. sativa*
Phenology & turnover			
Transfer growth period (% growing season)	0.2	0.3	1
Litter fall period (% growing season)	0.2	0.2	1
Leaf & fine root turnover fraction ($year^{-1}$)	1	0.32	1
Live wood turnover fraction ($year^{-1}$)	0.07	0.07	/
Whole plant mortality fraction ($year^{-1}$)	0.005	0.02	0.1
Allocation & N requirement			
New fine root C/new leaf C	1	0.78[a]	1
New stem C/new leaf C	2.2	1.74	3.0[b]
New live wood C/new total wood C	0.209	0.1	/
New root C/new stem C	0.22	0.29	/
Current growth proportion (%)	0.5	0.5	0.5
Leaf C/N	28.6[c]	25[a]	12.89[d]
Leaf litter C/N	32.2	75	45
Fine root C/N	48	21.79[a]	19.5[d]
Live wood C/N	50	50	/
Dead wood C/N	550	550	/
Leaf litter labile proportion	0.38	0.29[a]	0.64[e]
Leaf litter cellulose proportion	0.44	0.52[a]	0.25[e]
Leaf litter lignin proportion	0.18	0.19[a]	0.12[e]
Fine root labile proportion	0.34	0.34	0.34
Fine root cellulose proportion	0.44	0.44	0.44
Fine root lignin proportion	0.22	0.22	0.22
Dead wood cellulose proportion	0.68	0.71	/
Dead wood lignin proportion	0.32	0.29	/
Canopy parameter			
Canopy water interception coefficient (1/LAI/d)	0.045	0.1[f]	0.12
Canopy light extinction coefficient	0.54	0.55	0.85[b]
All-sided to projected leaf area ratio	2	2.3	2
Canopy average specific leaf area (m^2/kgC)	27.92[g]	34.1[f]	31.0[f]
Shaded SLA/Sunlit SLA	2	2	2
Fraction of leaf N in Rubisco	0.14	0.04	0.21
Maximum g_s ($m\ s^{-1}$)	0.006	0.006	0.006
Cuticular conductance ($m\ s^{-1}$)	0.00006	0.00006	0.00006
Boundary layer conductance ($m\ s^{-1}$)	0.01	0.02	0.04
VPD: start of g_s reduction (Pa)	1000[h]	970	930
VPD: complete g_s reduction (Pa)	4000[h]	4100	4100

Abbreviations: C = carbon; N = nitrogen; LAI = leaf area index; SLA = specific leaf area; g_s = stomatal conductance; [a] = Xu et al. (2001); [b] = Bai and Bao (2002); [c] = Zheng & Shangguan (2006); [d] = Ding et al. (1996); [e] = Bai et al. (1999); [f] = Xia and Shao (2008); [g] = Song et al. (2013); [h] = Bon-Lamberty et al. (2005).

Table 2 Accuracy of estimated annual evapotranspiration by the modified Biome-BGC model for *Robinia pseudoacacia*, *Caragana korshinskii*, and *Medicago sativa*.

Species	MD (mm)	RMSE (mm)	MAPE (%)
R. pseudoacacia	9.49	51.08	9.54
C. korshinskii	19.89	59.76	15.62
M. sativa	17.62	52.20	10.50

Table 3 Simulated actual evapotranspiration (AET), net primary productivity (NPP) and maximum leaf area index (LAI) of *Robinia pseudoacacia*, *Caragana korshinskii*, and *Medicago sativa* in three rainfall zones.

Species	Rainfall zone	*n*	AET (mm)	Max. LAI	NPP (g C m^{-2} yr^{-1})
R. pseudoacacia	>550 mm	68	554.0 ± 35.5	3.1 ± 0.2	551.3 ± 30.1
	450–550 mm	90	473.0 ± 37.5	2.7 ± 0.3	489.1 ± 60.6
	<450 mm	85	384.6 ± 37.3	2.0 ± 0.3	357.4 ± 59.4
C. korshinskii	>550 mm	68	550.1 ± 33.3	2.1 ± 0.1	181.7 ± 12.0
	450–550 mm	90	470.0 ± 37.5	1.9 ± 0.2	158.7 ± 18.8
	<450 mm	85	384.4 ± 38.0	1.4 ± 0.2	121.6 ± 19.1
M. sativa	>550 mm	68	554.0 ± 35.4	2.0 ± 0.5	165.8 ± 44.8
	450–550 mm	90	471.7 ± 36.3	1.2 ± 0.3	100.5 ± 25.8
	<450 mm	85	385.5 ± 35.4	0.9 ± 0.1	74.5 ± 6.5

Table 4 Pearson correlation coefficient between mean AET, maximum LAI, mean NPP and climate variables, soil texture and elevation for the three selected plants in the Loess Plateau.

Variable	Species	MAP	MAT	ELV	CC	SL	SA
	R. pseudoacacia	0.999**	0.592**	–0.502**	0.677**	0.497**	–0.592**
AET	*C. korshinskii*	0.978**	0.639**	–0.561**	0.655**	0.485**	–0.576**
	M. sativa	0.997**	0.613**	–0.520**	0.680**	0.496**	–0.593**
	R. pseudoacacia	0.923**	0.400**	–0.350**	0.664**	0.475**	–0.572**
LAI	*C. korshinskii*	0.794**	0.736**	–0.789**	0.440**	0.296**	–0.365**
	M. sativa	0.774**	0.895**	–0.750**	0.573**	0.346**	–0.446**
	R. pseudoacacia	0.924**	0.406**	–0.356**	0.665**	0.475**	–0.572**
NPP	*C. korshinskii*	0.796**	0.742**	–0.793**	0.443**	0.298**	–0.368**
	M. sativa	0.772**	0.895**	–0.748**	0.574**	0.349**	–0.449**

Note: AET = actual evapotranspiration; LAI = leaf area index; NPP = net primary productivity; MAP = mean annual precipitation; MAT = mean annual temperature; CC = clay content; SL = silt content; SA = sand content; ELV = elevation; ** = Significant at $p < 0.001$ (2-tailed).

Table 5 Step-wise regression for the main variables driving spatial distribution of mean NPP of each of the investigated plant species in the Loess Plateau.

Species	Regression equation	R^2	F	P	n
R. pseudoacacia	NPP=1.22×MAP–15.34×MAT+2.83×CC–0.04×ELV+53.27	0.895	507.06	0.000**	243
C. korshinskii	NPP=0.21×MAP–3.78×MAT+0.20×SL–0.05×ELV+133.94	0.855	350.67	0.000**	243
M. sativa	NPP=0.26×MAP+18.11×MAT–0.62×SL+0.03×ELV–187.86	0.913	622.72	0.000**	243

Note: NPP = net primary productivity; MAP = mean annual precipitation; MAT = mean annual temperature; CC = clay content; SL = silt content; ELV = elevation; ** = significance at $p < 0.001$.